Published OnlineFirst October 17, 2018; DOI: 10.1158/1541-7786.MCR-18-0440



Molecular Cancer Research

# Genetic and Epigenetic Determinants of Aggressiveness in Cribriform Carcinoma of the Prostate

Habiba Elfandy[1,2], Joshua Armenia[3], Filippo Pederzoli[4], Eli Pullman[5], Nelma Pertega-Gomes[1], Nikolaus Schultz[6], Kartik Viswanathan[7], Aram Vosoughi[7,8], Mirjam Blattner[8,9], Konrad H. Stopsack[10], Giorgia Zadra[1,11], Kathryn L. Penney[12,13], Juan Miguel Mosquera[7,8], Svitlana Tyekucheva[14,15], Lorelei A. Mucci[12], Christopher Barbieri[8,9], and Massimo Loda[1,11,16]

## Abstract

Among prostate cancers containing Gleason pattern 4, cribriform morphology is associated with unfavorable clinicopathologic factors, but its genetic features and association with long-term outcomes are incompletely understood. In this study, genetic, transcriptional, and epigenetic features of invasive cribriform carcinoma (ICC) tumors were compared with non-cribriform Gleason 4 (NC4) in The Cancer Genome Atlas (TCGA) cohort. ICC ($n = 164$) had distinctive molecular features when compared with NC4 ($n = 102$). These include: (i) increased somatic copy number variations (SCNV), specifically deletions at 6q, 8p and 10q, which encompassed *PTEN* and *MAP3K7* losses and gains at 3q; (ii) increased $SPOP^{mut}$ and $ATM^{mut}$; (iii) enrichment for *mTORC1* and *MYC* pathways by gene expression; and (iv) increased methylation of selected genes. In addition, when compared with the metastatic prostate cancer, ICC clustered more closely to metastatic prostate cancer than NC4. Validation in clinical cohorts and genomically annotated murine models confirmed the association with $SPOP^{mut}$ ($n = 38$) and $PTEN^{loss}$ ($n = 818$). The association of ICC with lethal disease was evaluated in the Health Professionals Follow-up Study (HPFS) and Physicians' Health Study (PHS) prospective prostate cancer cohorts (median follow-up, 13.4 years; $n = 818$). Patients with ICC were more likely to develop lethal cancer [HR, 1.62; 95% confidence interval (CI), 1.05–2.49], independent from Gleason score (GS).

**Implications:** ICC has a distinct molecular phenotype that resembles metastatic prostate cancer and is associated with progression to lethal disease. *Mol Cancer Res; 1–11. ©2018 AACR.*

## Introduction

Despite advances in biomarker discoveries and molecular testing, the Gleason grading system plays a significant role in the prognosis of prostate cancer outcomes and in clinical decisions (1). It is based on basic grade patterns depicted in a standard scheme to generate the final grade (sum of the dominant and next most common patterns). Recently, from the original Gleason grading, a simplified five-tiered grading system has emerged. This new grading was found to reflect the tumor behavior more reliably than the original Gleason score (GS; ref. 2).

Among Gleason grades, there is a growing interest in the role played by prostatic cancer with Gleason pattern 4 in terms of aggressive disease, for example, a single focus of GS 4 is sufficient for a patient to be excluded from active surveillance and placed into a definitive treatment protocol, usually surgery or radiation (3). Cribriform growth pattern has attracted attention because of the observed unfavorable biologic behavior. In the original Gleason description, cribriform glands used to be distributed between GS3 and GS4 (4), but cribriform is currently represented exclusively in GS4 (2). The presence of a cribriform component has been associated with poorer prognosis when compared with cases without cribriform pattern of the same GS (5). Tumors with cribriform morphology are more often associated with unfavorable clinicopathologic factors, including higher tumor volume, higher GS, extracapsular spread, positive resection margin, and biochemical

[1]Department of Oncologic Pathology, Dana-Farber Cancer Institute, Boston, Massachusetts. [2]Department of Pathology, National Cancer Institute, Cairo University, Cairo, Egypt. [3]Marie-Josée and Henry R. Kravis Center for Molecular Oncology, Memorial Sloan Kettering Cancer Center, New York, New York. [4]Vita-Salute San Raffaele University, Milan, Italy. [5]George Washington University, Washington, D.C. [6]Memorial Sloan Kettering Cancer Center, New York, New York. [7]Department of Pathology, Weill Cornell Medicine, New York, NY, USA. [8]Englander Institute for Precision Medicine, Weill Cornell Medicine, New York, New York. [9]Department of Urology, Weill Cornell Medicine, New York, New York. [10]Department of Medicine, Memorial Sloan Kettering Cancer Center, New York, New York. [11]Department of Pathology, Brigham and Women's Hospital, Harvard Medical School, Boston, Massachusetts. [12]Department of Epidemiology, Harvard T.H. Chan School of Public Health, Boston, Massachusetts. [13]Department of Medicine, Channing Division of Network Medicine, Brigham and Women's Hospital and Harvard Medical School, Boston, Massachusetts. [14]Biostatistics and Computational Biology, Dana-Farber Cancer Institute, Boston, Massachusetts. [15]Department of Biostatistics, Harvard TH Chan School of Public Health, Boston, Massachusetts. [16]The Broad Institute, Cambridge, Massachusetts.

**Note:** Supplementary data for this article are available at Molecular Cancer Research Online (http://mcr.aacrjournals.org/).

**Corresponding Author:** Massimo Loda, Dana-Farber Cancer Institute, Brigham and Women's Hospital, The Broad Institute, 450 Brookline Ave., Boston, MA 02215. Phone: 617-632-4001; Fax: 617-632-4005; E-mail: massimo_loda@dfci.harvard.edu

**doi:** 10.1158/1541-7786.MCR-18-0440

Published OnlineFirst October 17, 2018; DOI: 10.1158/1541-7786.MCR-18-0440



recurrence (BCR) after prostatectomy, reviewed previously (1). Moreover, two prior retrospective studies have reported associations with risk of metastasis (5, 6). Recently, cribriform morphology has been integrated into the Rotterdam European Randomized Study of Screening for Prostate Cancer Risk Calculator to predict high-risk prostate cancer (7). Associations of ICC and prognosis were observed in tumors with any quantity of ICC, irrespective of GS and tumor stage, indicating that focal/minor components should be regarded as clinically relevant (8, 9).

The Cancer Genome Atlas (TCGA) provides an unprecedented look into the molecular features of primary prostate cancer. A recent analysis of TCGA identified eight subtypes defined by a single molecular driver, namely, a gene fusion (*ERG*, *ETV1*, *ETV4*, and *FLI1*), a mutation (*SPOP*, *FOXA1*, and *IDH1*), or "other" for patients that did not fall into the previous seven subtypes (10). The motivation for defining such subtypes was to utilize them for clinical application.

Our aim in this study was to define the molecular features of cribriform carcinoma using TCGA cohort and compare it to that of GS4 noncribriform pattern tumors and ultimately to that of metastatic disease (11). We also aimed to assess the association between cribriform morphology and development of lethal outcomes in prospective cohorts of patients with primary prostate cancers. This study highlighted the genomic and methylation changes, transcriptionally deregulated biologically important pathways and molecular similarities with metastatic prostate cancer. We also validated the prognostic significance of ICC in large prospective cohorts with long-term follow-up.

## Materials and Methods

### TCGA and SU2C/PCF Dream Team prostate cancer cohorts

The publicly available TCGA (10) and SU2C/PCF Dream Team (11) prostate cancer cohorts were analyzed (12, 13). Somatic copy number variation (SCNV), mutation, and clinical data were retrieved directly from cBioPortal, and Level 3 mRNA expression and methylation data were downloaded from FireHose (https://gdac.broadinstitute.org). Copy number alteration was defined in each gene by sample-specific threshold as follows: deep deletion (−2), shallow deletion (−1), neutral (0), gain (+1), and amplification (+2) in Genomic Identification of Significant Targets in Cancer (GISTIC) analysis (12, 13).

### Classifying the TCGA cases into cribriform and noncribriform

Images of the scanned frozen sections of primary prostate cancer (10) were rereviewed with the intent to identify invasive cribriform carcinoma (ICC) pattern on the slide representing the block on which the molecular analyses were done. We assessed the samples according to the 2014 International Society of Urological Pathology (ISUP) updates (2) whereby all ICC patterns (small, large, regular, and irregular solid masses punctuated by round lumina with no intervening stroma) have been categorized as GS4 (Supplementary Fig. S1). Cases were considered ICC when the cribriform invasive pattern was ≥5% of tumor in the examined section(s). We evaluated the images with stringent adherence to the histomorphologic criteria for differentiation from other mimics, for example, high-grade prostate intraepithelial neoplasia (HGPIN). No attempt was made to distinguish ICC from intraductal carcinoma because of their comparable prognostic impact and the inability to distinguish between the two (5, 6, 8) as the blocks were not available for IHC. Two cases with extensive freezing artifacts were excluded because of difficulty in assigning GS. Prior to analysis, we excluded any sample lacking the GS4 component, that is, 3 + 3 and 5 + 5 (Supplementary Fig. S2). Ultimately, 266 patients with Gleason 4 component in TCGA were analyzed; ICC ($n = 164/266$, 62%) and NC4 ($n = 102/266$, 38%; IDs are provided in Supplementary Table S1).

### Health Professionals Follow-up Study and Physicians' Health Study prospective prostate cancer cohorts

Health Professionals Follow-up Study (HPFS) is an ongoing prospective cohort study of initially 51,529 men that has been followed with biannual questionnaires since 1986 (14). Physicians' Health Study (PHS) is a prospective cohort study of initially 29,067 men that started as primary prevention trials of aspirin and vitamin supplements with start of annual follow-up in 1982 and 1999 (15, 16). Incident prostate cancer diagnosed and self-reported during follow-up of HPFS/PHS was confirmed with the review of medical records and pathology reports. Follow-up for lethal cancer, defined as development of metastases and prostate cancer–specific death, occurred through specific questionnaires to the patients with prostate cancer, contact to treating physicians, review of medical record, and death certificates. Follow-up for mortality is >98% complete.

Archival formalin-fixed paraffin-embedded specimens from radical prostatectomy and transurethral resection of the prostate (TURP) were retrieved from treating hospitals, described elsewhere (17). All samples were centrally rereviewed by genitourinary pathologists, including centralized GS (18) with the majority being updated to the 2014 grading system (2). Tissue microarrays (TMA) were constructed using at least three 0.6-mm tumor cores per patient from the primary nodule or the nodule with the highest GS. We evaluated hematoxylin and eosin slides from 14 TMAs for the presence of ICC. Samples with cribriform component in one of the cores were considered ICC, without any cutoff for the proportion of tumor area. TMAs were additionally evaluated for PTEN protein expression, as described previously (19, 20).

### Weill Cornell Medicine validation cohort

Whole-exome sequencing data from 118 unselected prostate cancer cases at Weill Cornell Medicine (WCM) were retrieved (21). Of these, 11 (9.3%) demonstrated *SPOP* mutation ($SPOP^{mut}$). Blinded to mutation status, we assessed all prostatectomy slides from the 11 $SPOP^{mut}$ and 11 *SPOP* wild-type ($SPOP^{wt}$) cases matched for GS and pathologic stage. Dominant and secondary tumor nodule(s) from each prostatectomy specimen were assessed for the presence or absence of ICC (≥5% cutoff). Furthermore, 49 prostate cancer cases from the well-characterized WCM cohort of the Early Detection Research Network (EDRN) were also reviewed (21, 22). Eight additional cases of $SPOP^{mut}$ prostate cancer and eight wild-type controls were included. At the end, 38 samples were used for the analysis ($n = 19$ $SPOP^{mut}$ and $n = 19$ $SPOP^{wt}$) and all samples were either GS 3 + 4 or 4 + 3. *SPOP* status for the WCM EDRN cohort was established by high-resolution melting (HRM) followed by Sanger sequencing confirmation (21). For all cases, data on *ERG* and *SPOP* status were available. Statistical analysis was performed to look for an association between ICC and *SPOP* status.

### Mouse model

We utilized a previously developed transgenic mouse model with prostate-specific SPOP-F133V expression, Rosa26SPOP/SPOP mice crossed with PbCre4;$Pten^{L/+}$ mice for validation,

Published OnlineFirst October 17, 2018; DOI: 10.1158/1541-7786.MCR-18-0440



described previously (23). Blinded to the genotype, we assessed the morphology for presence or absence of cribriform morphology in 56 mice with the following genotypes: 4 $PTEN^{+/+}/SPOP^{wt}$, 4 $PTEN^{+/+}/SPOP^{mut}$, 11 $PTEN^{L/L}/SPOP^{wt}$, 12 $PTEN^{L/L}/SPOP^{mut}$, 15 $PTEN^{L/+}/SPOP^{mut}$, and 10 $PTEN^{L/+}/SPOP^{wt}$.

### Statistical analysis

Statistical analysis was performed by using IBM SPSS statistical version 23, Qlucore Omics Explorer R, and SAS 9.4 (SAS Institute). The threshold for statistical significance was set at $P < 0.05$ (two-sided). Correction for multiple testing was performed using Benjamini–Hochberg FDR. FDR (q-value) of 0.05 was considered significant. Categorical clinicopathologic variables and TCGA clusters were described by frequency and percentage and the comparisons were carried out by $\chi^2$ test. Mann–Whitney and Kruskal–Wallis nonparametric tests were used to assess the difference in fraction genomic altered (FGA) between ICC and NC4 as well as between GS, respectively. The comparison of individual SCNV between ICC and NC4 was done using Fisher exact test. Multivariable logistic regression was performed to assess whether SCNVs were associated with ICC when adjusting for FGA (continuous) and GS (categorical: 3 + 4, 4 + 3, ≥8). For the gene expression analysis, we used the moderated *t* test approach as implemented by *limma* package and the genes were considered differentially expressed on the basis of q value < 0.05 and $|\log_2$ fold change$| > 0.5$. Gene Set Analysis (GSA) was carried out using Bioconductor package *limma* for the functional annotation of the differentially expressed genes by using 3 gene sets collection from the Molecular Signature Database (MsigDB): Gene Ontology (GO) biological processes (24), Kyoto Encyclopedia of Genes and Genomics (KEGG; ref. 25), and Hallmark (26). Methylation data were obtained from FireHose and the annotations from Illumina website. The probes not having any missing values (386,741 probes) were considered in the analysis. Methylation threshold was set at beta of 0.2 (≥0.2 was considered methylated). Differential methylation was assessed statistically using Fisher exact and $\chi^2$ test with q-value <0.05. SCNVs of ICC were then compared with metastatic prostate cancer in the Stand Up To Cancer/Prostate Cancer Foundation Dream Team cohort (SU2C) by cluster analysis. The HPFS/PHS prostate cancer cohorts were combined for analysis, including 818 cases with any pattern 4 (i.e., 3 + 4 to 9). The association of GS (ordinal) and ICC was assessed using logistic regression. *PTEN* status was dichotomized as complete loss in contrast to intact expression in any tumor core (Supplementary Fig. S3). To assess the associations of *PTEN* status with ICC, we used logistic regression with and without adjustment for GS (categorical: 3 + 4, 4 + 3, 8, and 9). To assess the association of ICC and time from cancer diagnosis to lethal cancer, we used Cox proportional hazards regression stratified by or adjusted for GS. Models were additionally adjusted for age at diagnosis (linear) and body mass index (BMI; categorical: <25, 25–30, and >30 kg/m$^2$). In a separate model, we also adjusted for clinical tumor stage (categorical: T1/T2 N0/Nx M0/Mx, T3 N0/Nx M0/Mx, and T4 N1 M1), a probable intermediate between morphology and lethal disease. To test whether the association of ICC and lethal disease differed by GS, a multiplicative interaction term was tested. Proportionality of hazards was assessed using weighted Schoenfeld residuals and interactions with follow-up time, there were no departures. *P* values were two-sided.

## Results

### Clinicopathologic features of ICC in TCGA dataset

The prevalence of ICC, in the selected cases as described above, was 62% ($n = 164/266$). As expected, ICC was significantly associated with high GS (GS ≥ 8), higher tumor stage, and lymph node metastases in the localized tumors. No association was found between ICC and age, preoperative PSA, and ethnic group (data not shown). Demographic and clinicopathologic factors are summarized (Table 1; Supplementary Fig. S4).

### Distribution of ICC cases within TCGA molecular classes and clusters

Seven molecular classes were identified in the original TCGA cohort based on oncogenic drivers, namely: *ERG*, *ETV1*, *ETV4*, *FLI1*, *SPOP* mutation, *IDH1* mutation, and *FOXA1* mutation. The prevalence of ICC compared with NC4 in *SPOP* mutation class was 90.3% versus 9.7%, ($n = 28/31$ vs. $n = 3/31$, $P < 0.001$). No association was found between ICC and other molecular classes. There were differences between ICC and NC4 with respect to

**Table 1.** Clinicopathologic variables of TCGA and HPFS/PHS cohorts

| | TCGA | | HPFS/PHS | |
|---|---|---|---|---|
| | **ICC** $n = 164$ **(62%)** | **NC4** $n = 102$ **(38%)** | **ICC** $n = 218$ **(27%)** | **NC4** $n = 600$ **(73%)** |
| GS | | | | |
| 3 + 4 | 55 (33.5) | 23 (22.5) | 48 (22.0) | 334 (55.7) |
| 4 + 3 | 39 (23.8) | 63 (61.8) | 76 (34.9) | 165 (27.5) |
| 8 | 36 (21.95) | 9 (8.8) | 43 (19.7) | 35 (5.8) |
| 9 | 34 (20.7) | 7 (6.9) | 51 (23.4) | 66 (11.0) |
| Tumor pathologic stage (pT) | | | | |
| NA | 2 (1.2) | 1 (1) | 20 (9.2) | 37 (6.2) |
| pT1/2 | 38 (23.17) | 45 (44) | 111 (50.9) | 400 (66.7) |
| pT3 | 77 (46.95) | 48 (47) | 75 (34.4) | 145 (24.2) |
| pT4/N1/M1 | 47 (28.7) | 8 (7.8) | 12 (5.5) | 18 (3.0) |
| PTEN status (IHC) | | | | |
| NA | – | – | 43 (19.7) | 126 (21.0) |
| Complete loss | – | – | 47 (21.6) | 75 (12.5) |
| Intact, any core | – | – | 128 (58.7) | 399 (66.5) |
| Outcome | | | | |
| Nonlethal | – | – | 175 (80.3) | 554 (92.3) |
| Lethal | – | – | 43 (19.7) | 46 (7.7) |

Abbreviation: NA, not available.

Published OnlineFirst October 17, 2018; DOI: 10.1158/1541-7786.MCR-18-0440



TCGA clusters, defined by miRNA, copy number, reverse protein arrays (RPPA), DNA methylation profiles, and TCGA integrative cluster (iCluster; Supplementary Table S2). ICC was associated with increased occurrence of SCNV expressed as a fraction of altered genome ($P < 0.001$) and dominated methylation clusters 1 and 2 that are characterized by increased DNA promoter methylation ($P = 0.001$).

### SCNVs and mutations in ICC

***Overall genome alteration and SCNVs.*** In contrast to other solid tumors, prostate cancer is known to orchestrate its molecular alteration mainly by SCNV (27). To explore the copy number profile of ICC pattern, we compared SCNVs between ICC and NC4. After excluding the events with low frequency (<5%), we analyzed a total of 450 gains and 551 losses. As expected, FGA was significantly higher in ICC compared with NC4 ($P < 0.001$). High GS were also associated with FGA ($P < 0.001$), implying that FGA is possibly associated with ICC through GS (Supplementary Fig. S5). Therefore, analyses for individual SCNVs were adjusted for FGA and GS. Out of the 208 significantly associated copy number aberrations ($q < 0.15$), only 51 SCNV events were independently associated with ICC after the adjustment for FGA and GS. Notably, shallow deletions and gains were driving the significance (Fig. 1A and B). The most common losses were identified at 8p ($P = 0.001$), 6q ($P = 0.03$), and 13q ($P = 0.01$) and the most frequent gains were at 3q ($P < 0.001$) and 3p ($P = 0.03$; Fig. 1C). After the adjustment for GFA and GS, ICC remained significantly associated with deletions at 8p21–22, 6q21, 11q22–23, and 10q23 and gains at 3q11–29 (Supplementary Table S3). Deletions at 8p were considered an independent prognosticator in prostate cancer (28). It was reported to be the second most frequent aberration after *ERG fusion*, accounting for 55% and 90% in primaries and advanced prostate cancer, respectively (29). The observed SCNVs in ICC span large chromosomal regions harboring several tumor suppressor genes (TSG) known to play a crucial role in prostate cancer, for example, *PTEN* (10q23.3, 39%), *NKX3-1* (8p21.2, 72.56%), and *MAP3K7* (6q15, 45.7%). *PTEN* is a frequently altered TSG in prostate cancer and is associated with poor outcome (20, 30). $PTEN^{loss}$ was significantly enriched in ICC [39%, $n = 64/164$ vs. 25.5%, $n = 24/102$; OR = 1.87; 95% confidence interval (CI), 1.09–3.26; $P = 0.024$, $q = 0.13$]. This association with ICC was also significant in PTEN homozygous loss (23%, $n = 38/164$ vs. 10.7%, $n = 11/102$; OR = 2.52; 95% CI, 1.23–5.26; $P = 0.014$; Fig. 1A). *NKX3*-1, a prostate-specific TSG that enhances DNA repair by ATM activation (31), was suppressed in 40%–80% of the castration-resistant prostate cancers (CRPC; ref. 27). In ICC, NKX3-1 was the most common deletion (72.56%, $n = 119/164$). Moreover, ICC is enriched for aberrations previously correlated with aggressive behavior, for example, *GATA2*, *PRKCI*, and *PIK3CA/B* (Supplementary Table S4). Some of these SCNVs are correlated with gene expression (Table 2).

### Mutations

A total of 825 mutations were found. The top five ranked mutations, according to their frequency, were *ERG fusion*, *SPOP*, *TTN*, *ETV1*, and *TP53* (Supplementary Table S5). When compared, *SPOP* and *ATM* mutations (two DNA-repair genes) were significantly higher in ICC than in NC4; $SPOP^{mut}$ (17.1%, $n = 28/164$ vs. 2.9%, $n = 3/102$; OR = 6.79; 95% CI, 2.18–21.67; $P < 0.001$; q = 0.003) and $ATM^{mut}$ (7.3%, $n = 12/164$ vs. 0.98%, $n = 1/102$; OR = 7.97; 95% CI, 1.21–86.33; $P = 0.019$; q = 0.1; Fig. 1B and D). *ERG fusion*, the most frequent genetic abnormality in prostate cancer, was not different between ICC and NC4 (46.3%, $n = 76/164$ vs. 47.1%, $n = 48/102$; OR = 0.97, 95% CI, 0.6–1.57; $P = 0.99$).

***Key aberrations in ICC.*** As mentioned above, the ICC tumors were enriched for several genes known to play a critical role in prostate cancer, but the most interesting ones are $PTEN^{loss}$ and $SPOP^{mut}$ due to two main reasons. First, $SPOP^{mut}$ and $PTEN^{loss}$ are statistically more likely to occur in ICC than in NC4. When adjusted for GS, these associations remained significant; $PTEN^{loss}$ (OR = 1.91; 95% CI, 1.05–3.52; $P = 0.03$) and $SPOP^{mut}$ (OR = 5.54; 95% CI, 1.78–24.4; $P = 0.008$). Second, $PTEN^{loss}$ and $SPOP^{mut}$ have been previously regarded as distinct molecular groups on their own: $PTEN^{loss}$ has emerged as a distinct group with worse clinical outcome (30, 32). In addition, in a meta-analysis study, $PTEN^{loss}$ was strongly linked to marked increase in SCNVs with wide involvement of the genome, including deletions at 8p and 13q (29). Remarkably, 8p and 13q are the most frequent deletions in ICC samples (Fig. 1C). However, after the adjustment for FGA and GS, the deletions at 13q were no longer significantly associated with ICC. In ICC, $PTEN^{loss}$ was associated with 8p deletion, albeit nonsignificantly. $SPOP^{mut}$, the most common mutation in prostate cancer, designates a distinct *ERG fusion*–negative class (33). In primary tumors, $SPOP^{mut}$ was reported to be inversely correlated to $PTEN^{loss}$ and frequently associated with *CHD1* and *MAP3K7* codeletions (33–35). Combined deletions of *CHD1* and *MAP3K7* were previously correlated with unfavorable outcome and reported in 10%–20% and 20%–25% of the primary and metastatic prostate cancers, respectively (36).

In agreement with these studies, we also found significant enrichment in ICC for $SPOP^{mut}$ associated with $CHD1^{loss}$ ($P < 0.001$) and 6q deletions encompassing $MAP3K7^{loss}$ ($P < 0.001$). Despite the observed codeletion of *CHD1* and *MAP3K7*, the adjustment for FGA and GS did not change the association between ICC and $MAP3K7^{loss}$ (OR = 2.73; 95% CI, 1.5–5; $P < 0.001$; q = 0.01; after adjustment OR = 2.26; 95% CI, 1.22–4.28; $P = 0.011$; q = 0.11). However, $CHD1^{loss}$ was no longer statistically significant (OR = 2.4; 95% CI, 1.13–5.5; $P = 0.021$, q = 0.12; after adjustment OR = 1.8; 95% CI, 0.8–4; $P = 0.16$). As previously reported, $PTEN^{loss}$ and $SPOP^{mut}$ were mutually exclusive in ICC ($P < 0.001$). Of interest, $PTEN^{loss}$ and $SPOP^{mut}$ together span 56% of ICC compared with 16.9% in NC4.

In summary, we showed that two genomic insults define two molecular subgroups in ICC: (i) $SPOP^{mut}$, which is associated with *CHD1* and *MAP3K7* codeletions; and (ii) $PTEN^{loss}$, which is mutually exclusive with $SPOP^{mut}$ (Fig. 1E).

### Comparison of gene expression and methylation patterns in ICC and NC4

***Gene expression profile.*** To identify the potential pathways that might emerge from changes in mRNA expression influenced by copy number and mutational insults, we performed gene set enrichment analysis. We detected 2,813 differentially expressed genes between ICC and NC4 with q < 0.05. Out of those, 1,009 also passed our log fold change (FC) threshold of $|\log FC| > 0.5$. Of these, 861 were underexpressed, whereas 148 were overexpressed in ICC (Supplementary Table S6). Among the overexpressed pathways in ICC, the functional pathways were involved in cell division, cell-cycle regulation, DNA replication, chromatin and histone modification, and transcriptional initiation (q < 0.05).

Published OnlineFirst October 17, 2018; DOI: 10.1158/1541-7786.MCR-18-0440



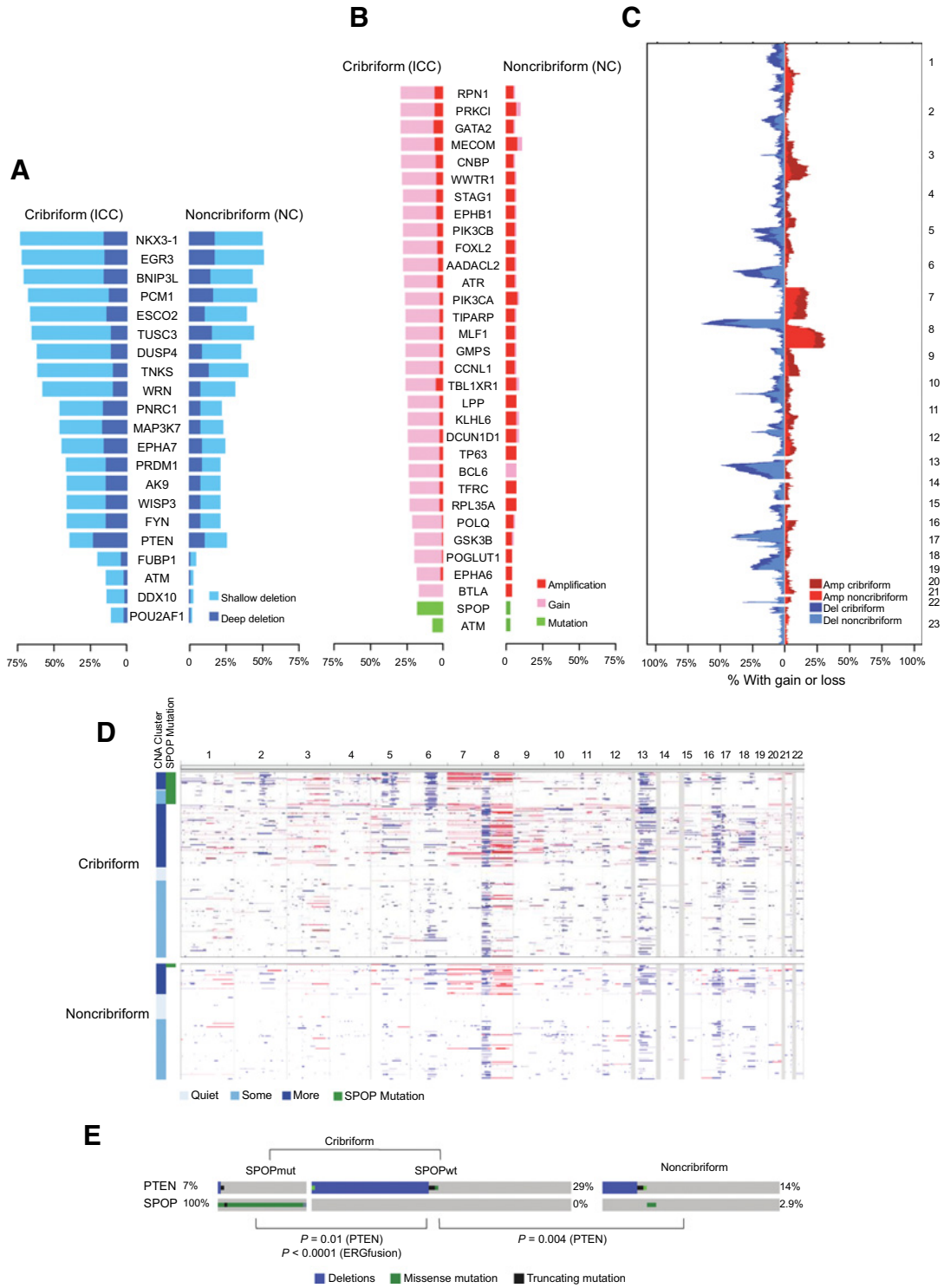


**Figure 1.**

Frequency (%) of the SCNV in ICC and NC4. ICC is significantly higher in SCNV events. **A,** Dark-blue represents deep deletions, light-blue represents superficial deletions. **B,** Red represents amplifications, magenta represents gains, and green represents mutations. The SCNVs in **A** and **B** are the adjusted events for FGA and GS. **C,** Landscape of copy number alterations in ICC and NC4: The chromosomes are displayed horizontally and the frequency is displayed on the *y*-axis. **D,** Distribution of SCNV clusters and *SPOP* mutation within each ICC and NC4 groups (164 and 102 samples, respectively). In the column sidebar of the figure, blue represents the SCNV clusters and green represents $SPOP^{mut}$ groups. In the heatmap, red represents gains/amplifications and blue represents deletions. Chromosomes are represented in columns and samples are represented in rows. **E,** The frequency of $SPOP^{mut}$ and $PTEN^{loss}$ in ICC and NC4. The *P* values in **E** were derived considering deep deletions and mutations of *PTEN*.

Published OnlineFirst October 17, 2018; DOI: 10.1158/1541-7786.MCR-18-0440



**Table 2.** Differentially expressed genes (mRNA) between ICC and NC4 mapped to SCNV chromosomal regions enriched in ICC

| Gene | Cytoband | LogFC | q value |
|---|---|---|---|
| Gain and upregulation | | | |
| POLQ | 3q13.33 | 0.73 | 5.09E−05 |
| GATA2 | 3q21.3 | 0.24 | 2.49E−02 |
| GMPS | 3q24 | 0.2 | 2.38E−03 |
| ATR | 3q23 | 0.18 | 2.71E−02 |
| Deletion and downregulation | | | |
| BNIP3L | 8p21.1 | −0.24 | 4.13E−03 |
| PTEN | 10q23.3 | −0.4 | 5.76E−03 |
| POU2AF1 | 11q23.1 | −0.56 | 3.99E−02 |
| EGR3 | 8p23-p21 | −0.75 | 1.76E−02 |

Furthermore, *mTORC1* and *MYC* signaling pathways, had higher expression in ICC. Our results also indicated that angiogenesis, cell migration, epithelial–mesenchymal transition (EMT), cell–matrix adhesion, *MAPK*, *KRAS*, and *JAK–STAT* signaling pathways were significantly enriched in ICC (Supplementary Table S7). Interestingly, some of the genes constituting these pathways have been proposed as potential targets for prostate cancer therapy, for example, *BIRC5*, *PLK1*, *CDC45*, *FOXM1*, *CDCA3*, *and UHRF1* (Supplementary Table S8).

***Methylation profile.*** Prior studies in prostate cancer have shown that DNA methylation was more frequent than genomic insults in advanced and metastatic prostate cancer (37, 38). This has led us to analyze the methylation difference between ICC and NC4. We found 52 significantly hypermethylated genes (OR $\geq$ 3) and 22 hypomethylated genes (OR $\leq$ 0.33) in ICC with q < 0.05 (Supplementary Table S9). Unsupervised clustering of the 266 cases revealed two clusters based on different DNA-methylation levels, visualized in the heatmap (Fig. 2). ICC is enriched in the methylated cluster, whereas NC4 dominated the hypomethylated cluster. Unlike in a previous study of ICC methylation (39), we found a significant increase in methylation of *CYP26A1* in ICC but not of *APC*, RASSF1, and TBX15. Notably, several strongly methylated genes in ICC were correlated with reduced mRNA expression, such that the gene expression was differentially downregulated, for example, *ZNF853*, *DDIT4L*, *B3GAT1*, and *RASL12* (Supplementary Table S10). Interestingly, *EZH2* methyltransferase was transcriptionally overexpressed in ICC (logFC = 0.48, $q < 0.001$). *EZH2* overexpression has been implicated in prostate cancer progression. *TIMP2* and *TIMP3* (inhibitors of the tissue matrix, metalloproteinases) and *SLIT2* (inhibitor of chemotactic-induced cell migration), known downstream targets of *EZH2* in prostate cancer (40), were in fact repressed in ICC; *TIMP2* (logFC = −0.34, q = 0.013), *TIMP3* (logFC = −0.52, q < 0.001), and *SLIT2* (logFC = −0.46, q = 0.01). We observed a methylated CpG island shore of *TIMP2* in ICC (OR = 0.22; q = 0.01). Furthermore, among the differentially methylated genes that emerged from our analysis, we found a subset of genes that has been previously reported to be methylated and/or downregulated in aggressive prostate cancer, for example, *EVX1*, *EPHX3* (*ABHD9*), and *IRAK3* (Supplementary Table S11). Taken together, the results imply that the aggressive features of ICC could also be explained by epigenetic changes.

### Common features between ICC and metastatic prostate cancer based on SCNV and mutational status

The reported aggressive behavior of ICC (5, 6) led us to investigate the molecular features of ICC in comparison with

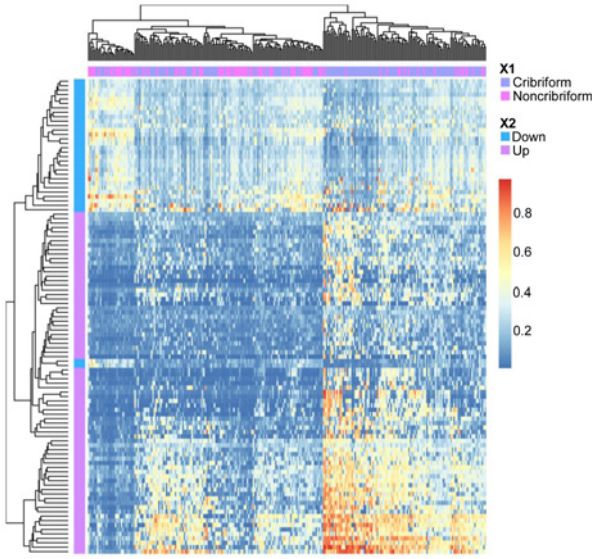


**Figure 2.**
Hierarchical clustering of 266 samples based on differentially methylated CpG islands between ICC and NC4. This figure shows the unsupervised hierarchical clustering analysis of ICC and NC4 (top) using differentially methylated CpG islands ($P < 0.01$ and $q < 0.05$). ICC samples dominate the hypermethylated cluster, whereas NC4 samples fell in the cluster with the lowest methylation level. Samples are represented in columns and genes in rows.

that of metastatic prostate cancer. From the independent SCNVs, in ICC, a binary matrix was created by including events with frequency >20% in ICC and q < 1.5 (Fig. 3). Then, unsupervised hierarchical clustering of combined genetic events in ICC, NC4, and metastatic prostate cancer was then performed. We identified four main clusters based on the frequency of genetic alteration. Clusters 1 and 2 each had a high frequency of SCNVs at 6q, 8p, and 3q. Metastatic and ICC samples constituted together 94% of cluster 1 and 100% of cluster 2. Deletions at 6q and 8p designate cluster 3 but no gains at 3q; metastatic and ICC samples comprised 75% of the cluster. Cluster 4 had the lowest frequency of SCNVs, where a subset of samples showed deletions at 6q and/or $PTEN^{loss}$ (40.6%), but 8p and 3q events are lacking. NC4 was dominantly condensed in cluster 4 representing 47.5% of its samples. Other common events, $PTEN^{loss}$ and $SPOP^{mut}$, were heterogeneous in their distribution between clusters. This could be explained by the effects imposed by the events at 8p and 3q in defining the clusters. These results indicate that, in contrast to NC4, ICC is genetically comparable with metastatic prostate cancer. This clustering pattern continues to support the clinically observed aggressive behavior and metastatic potential of ICC.

### Validation of ICC genetic alterations in external datasets (WCM and HPFS/PHS cohorts)

Finally, we validated our results from TCGA data using two independent external cohorts and a mouse model. We selected the two key alterations in ICC for validation, $PTEN^{loss}$, and $SPOP^{mut}$, discussed above.

***$PTEN^{loss}$ validation–human cohort.*** We evaluated 818 tumors for ICC in the HPFS/PHS cohorts. As expected, ICC was more common among tumors with higher GS, with 44% of GS9 tumor

Published OnlineFirst October 17, 2018; DOI: 10.1158/1541-7786.MCR-18-0440



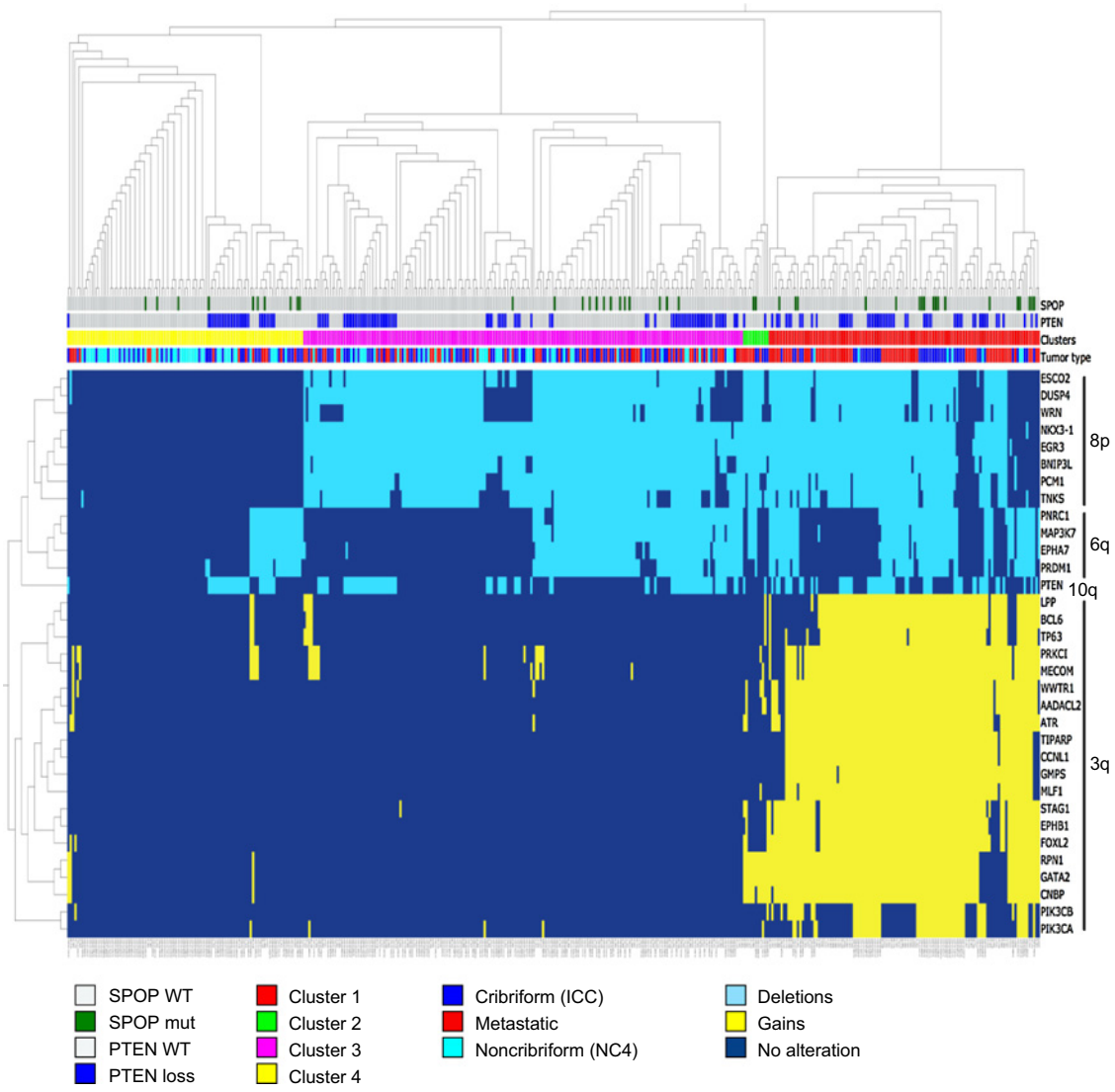


**Figure 3.**

Hierarchical clustering of integrated primary TCGA and metastatic prostate cancer datasets (266 and 150 samples, respectively) based on genetic alteration similarities. This figure shows the unsupervised clustering analysis of ICC, NC4, and metastatic using binary data of the independent SCNV events with frequency >20% in ICC (q < 0.1.5). The dendrogram demonstrates hierarchical separation into four clusters. ICC and metastatic are grouped mainly in clusters 1 and 2 ($n = 127$, both) that is characterized by the highest frequency of genetic alteration at 8p, 6q, and 3q. In cluster 1, ICC and metastatic samples constituted together 94.5% (37.8% and 56.9%, respectively), but comprised 100% of the cluster 2. Cluster 3 ($n = 188$) is enriched with ICC and metastatic samples (42% and 33%, respectively), designated by 6q and 8p aberrations. The lack of 3q and 8p distinguishes cluster 4 ($n = 101$) where NC4 samples are mainly condensed (47%). NC4 is minimally represented in cluster 1 and 2 (5.5%). Samples are displayed in columns and genes are represented in rows.

compared with 13% tumors with GS3 + 4 showing ICC ($P < 0.001$; Table 1). *PTEN* status was known for 649 tumors. Tumors with $PTEN^{loss}$ compared with those with intact *PTEN* expression were more likely to have ICC (39% vs. 24%; OR = 1.95; 95% CI, 1.29–2.96). However, when adjusting for GS, the association of $PTEN^{loss}$ and ICC was weaker and not statistically significant (OR = 1.38; 95% CI, 0.89–2.16). *SPOP* mutation status is not known in HPFS/PHS.

***$SPOP^{mut}$ validation–human cohort.*** The WCM cohort was comprised of GS7 (3 + 4 or 4 + 3) cases with 19 $SPOP^{mut}$ and 19 $SPOP^{wt}$ cases as control. ICC was observed in 53% ($n = 10/19$) of the $SPOP^{mut}$ samples, compared with 21% ($n = 4/19$) in $SPOP^{wt}$ samples ($P = 0.04$).

***$PTEN^{loss}$ and $SPOP^{mut}$ validation–mouse model.*** We assessed the contribution of $PTEN^{loss}$ and $SPOP^{mut}$ to cribriform morphology in a transgenic mouse prostate. $PTEN^{wt}$ with or without $SPOP^{mut}$ showed a normal morphologic prostate epithelium. $PTEN^{L/+}$ mice showed focal cribriform carcinoma only in the background of $SPOP^{mut}$, although this was not statistically significant. Cribriform morphology was observed in most $PTEN^{L/L}$ mice ($n = 18/23$), involving 15%–90% of the dorsolateral prostate (Supplementary Fig. S6). $SPOP^{mut}$ added more aggressive

Published OnlineFirst October 17, 2018; DOI: 10.1158/1541-7786.MCR-18-0440



**Table 3.** Lethal disease associated with ICC versus NC4 in the prospective prostate cancer cohorts within the HPFS and the PHS

| | NC4 | | | | ICC | | | |
|---|---|---|---|---|---|---|---|---|
| | Total | Lethal | (%) | HR[a] (95% CI[a]) | Total | Lethal | (%) | HR[a] (95% CI[a]) |
| Overall | 600 | 46 | 7.7 | | 218 | 43 | 19.7 | |
| Unadjusted | | | | 1 (ref.) | | | | 2.66 (1.75–4.03) |
| Model 1: + Gleason | | | | 1 (ref.) | | | | 1.62 (1.05–2.49) |
| Model 2: + Age, BMI | | | | 1 (ref.) | | | | 1.67 (1.08–2.59) |
| Model 3: + cTNM | | | | 1 (ref.) | | | | 1.45 (0.92–2.27) |
| By Gleason, unadjusted | | | | | | | | $P_{interaction} = 0.56$[b] |
| 3 + 4 | 334 | 10 | 2.9 | 1 (ref.) | 48 | 1 | 2.1 | 0.69 (0.09–5.38) |
| 4 + 3 | 165 | 17 | 10.3 | 1 (ref.) | 76 | 13 | 17.1 | 1.46 (0.71–3.02) |
| 8 | 35 | 7 | 20.0 | 1 (ref.) | 43 | 9 | 20.9 | 1.12 (0.42–3.00) |
| 9 | 66 | 12 | 18.2 | 1 (ref.) | 51 | 20 | 39.2 | 2.40 (1.17–4.93) |

Abbreviation: ref, reference category.
[a]HR with 95% CI.
[b]Interaction of cribriform morphology and Gleason grade (ordinal).

morphologic features to the $PTEN^{L/L}$ genotype in the form of less differentiated areas and sarcomatoid changes ($n = 5/12$), as described previously (23).

### ICC and lethal disease over long-term follow-up

Over a median follow up of 13.4 years, 89 of 818 patients in the prospective HPFS/PHS prostate cancer cohorts developed lethal cancer, defined as distant metastasis or cancer-specific mortality. Patients with ICC were 62% more likely than those without ICC to develop lethal disease after adjusting for GS (HR = 1.62; 95% CI, 1.05–2.49; $P = 0.028$). These estimates were attenuated when additionally adjusting for cancer stage (Table 3).

## Discussion

Because the behavior of GS4 tumors with cribriform morphology has been associated with aggressive clinical behavior, we set out to determine the key molecular features that would determine biologic aggressiveness characterizing this subtype of grade 4 prostate cancer, and to evaluate how the long-term prognosis of ICC differs when compared with NC4.

Our analysis shows that when compared with NC4 tumors, ICC tumors are more likely to have deletions at specific chromosomal sites, for example, 8p and 6q. These chromosomal regions harbor tumor suppressor genes known to play critical roles in prostate tumor development, progression, and therapy resistance. Many of these deletions were strongly correlated with aggressive behavior and early BCR, for example, *PTEN*, *NKX3-1*, *and MAP3K7*. In addition, $SPOP^{mut}$ and $ATM^{mut}$ are associated with ICC. These results outline that the most frequent genomic alterations with prognostic impact in prostate cancer are prevalent in ICC.

The associations of ICC with $SPOP^{mut}$ and $PTEN^{loss}$ remained significant after adjustment for GS in the TCGA data, but not in the HPFS/PHS (for $PTEN^{loss}$). Given that ICC evaluation was TMA-based, the results in this validation cohort could be attributed to sampling bias. $SPOP^{mut}$ status was not available in these cohorts. Because the complete analysis of all prostatectomy slides was not possible, we tested the sensitivity of TMA-based assessment for ICC by evaluating 25 full case slide sets and found a specificity of 100% (95% CI, 69–100) but a sensitivity of 71% (95% CI, 42–92). Although not being able to detect all ICC represents a limitation in our study, these results inform practice in the context of evaluating ICC in biopsy specimens.

In our mouse model bearing the $SPOP^{mut}$, $PTEN^{L/+}$ mice showed focal cribriform carcinoma only in the background of $SPOP^{mut}$. Although statistically not significant due to the limited number of mice, these findings suggest an association between $SPOP^{mut}$ and induction of a cribriform morphology in the mouse prostate.

Our GSA indicated that the cell cycle, replication, mitosis, and DNA-repair genes were enhanced, whereas cell adhesion and cell junction sets were suppressed in ICC. These results are in accordance with the known aggressiveness of ICC and may explain its metastatic potential. In addition, *MYC* and *mTORC1* pathways were upregulated, two main pathways activated in metastatic prostate cancer. The association of ICC with $PTEN^{loss}$ and $SPOP^{mut}$ further highlights the activation of *PI3K/mTOR* as a potentially relevant pathway in ICC. Indeed, $PTEN^{loss}$ is known to activate *PI3K/mTOR* pathway and it has recently been shown that $SPOP^{mut}$ can do the same (23, 41).

In this work, we were able to show the difference in DNA-methylation profile between ICC and NC4. The methylation changes affect genes related to BCR and prostate cancer progression. Recently, a study on ICC has assessed seven prognostic methylation biomarkers: *APC*, *CYP26A1*, *HOXD3*, *HOXD8*, *RASSF1*, *TBX15*, and *TGFβ2* (39). In their analysis, *APC*, *RASSF1*, and *TBX15* were hypermethylated in ICC. Of these, we only confirmed *CYP26A1* as being strongly methylated in ICC in the TCGA cohort. Importantly, *EZH2* was transcriptionally upregulated in ICC. Of interest, *EZH2* is a downstream target of *PI3K/mTOR* pathway, which triggered its methylation activity as documented in a cell culture study (42). These observations imply that the methylation changes in ICC are possibly *EZH2*-induced through the indirect contribution of $PTEN^{loss}$ and $SPOP^{mut}$ via the activation of *PI3K/mTOR* pathway. Altogether, these findings suggest that $PTEN^{loss}$ and $SPOP^{mut}$ not only contribute to the genomic stability, as reported in other studies, but can also influence the gene expression and methylation changes in ICC.

Finally, ICC and metastatic prostate cancer seem to display overlapping molecular features when directly compared. Cluster analysis demonstrated that ICC had similarities with metastatic prostate cancer in the SCNVs pattern, mainly gains at 3q, in addition to the deletions at 8p and 6q. These alterations likely

Published OnlineFirst October 17, 2018; DOI: 10.1158/1541-7786.MCR-18-0440



mediate the progression of ICC to metastatic disease more than others.

Although ICC was associated with oncogenic alterations, several aberrations offer therapeutic opportunities, for example, *PTEN*, *PI3KCA*, and *ATM*, reviewed in ref. 43. Likewise, *ATM and SPOP* mutations were found to be associated with responsiveness to DNA-damaging agents such as *PARP* inhibitors (34, 44).

Complementing the comprehensive analysis of the molecular genetic alterations that occur in ICC, we compared the long-term prognosis of ICC and NC4 tumors in the prospective HPFS/PHS cohorts. We found that localized cancers with ICC were considerably more likely to progress to lethal disease, independent of GS. Our results are in line with previous studies on ICC and BCR (8, 45), as well as retrospective and case–control studies that assessed the progression to metastatic disease (5, 6). Our analyses underscore the potential clinical importance of diagnosing and reporting the cribriform pattern on biopsy specimens as well as in radical prostatectomies. A recently proposed grading system stratifies prostate cancer into five grade groups. GS4 is a component of grade groups 2 (GS3 + 4), 3 (GS4 + 3), and 5 (GS4 + 5); the amount of Gleason grade 4 differentiates groups 2 and 3. Owing to the close association of ICC with aggressive molecular phenotypes and tumor lethality, our data show that ICC can subdifferentiate prognosis beyond grade groups.

Our results are consistent with the findings of a recent study of genome stability and SCNVs in ICC that used TCGA dataset and validated the results in Canadian Prostate Cancer Genome Network cohort (46). In their analyses, ICC was associated with 6q15, 8p21, loss of *PTEN, and NKX3–1* as well as $SPOP^{mut}$. In contrast to their results, we did not find an association with *RB1*, *TP53* deletions, *MYC* amplification, *FOXA1*, and *TP53* mutations. Discordant results could be attributed to differences in the threshold utilized to define the ICC component (5% in our analysis vs. 30% in theirs). Therefore, ICC constituted 62% of the TCGA samples in our analysis compared with 31% in their work. The cut-off rule we used ($\geq$5%) was reported to maintain the significant adverse prognostic association (8, 9), suggesting that our threshold is more reasonable in capturing most of ICC samples. The existing discrepancy between the two studies suggests the potential effect of ICC percentage on the molecular features. Addressing this point necessitates examining the whole tumor, whereas our study was limited to the available one tissue block. Moreover, we believe that fluid-based tests (e.g., serum and urine transcriptome, proteomics, and exosomes) would represent a better approach, as they provide a view of the genomic landscape of the whole tumor.

The importance of our work lies in its comprehensive approach. Our investigation outlines the copy number and mutational insults, methylation changes, deregulated biologically relevant pathways analyzed by the mRNA expression, and molecular similarities with metastatic/CRPC. We also verified the prognostic significance of ICC in a large prospective cohort with long-term follow-up.

The molecular insight gained in this study and other studies may assist in improving the diagnostic accuracy. Accounting for the potential sampling error in prostatic biopsies and limited visibility of ICC on multiparametric MRI (47), a biomarker that is indicative for the presence of ICC may be useful. Some of the aberrations in ICC could be traced in cell-free serum or urine DNA (48). This may open new avenues for considering fluid-based biopsies to triage patients before any further invasive intervention or to integrate into screening programs.

Our work has led us to conclude that the observed enrichment of a wide range of oncogenic alterations affecting tumor properties in ICC may confer a selective advantage to this subtype of Gleason grade 4 prostate cancer. This study also highlights the importance of ascribing molecular features to morphologic entities.

## Disclosure of Potential Conflicts of Interest

No potential conflicts of interest were disclosed.

## Authors' Contributions

**Conception and design:** H. Elfandy, F. Pederzoli, N. Pertega-Gomes, C. Barbieri, M. Loda

**Development of methodology:** H. Elfandy, F. Pederzoli, N. Pertega-Gomes, J.M. Mosquera, S. Tyekucheva, C. Barbieri, M. Loda

**Acquisition of data (provided animals, acquired and managed patients, provided facilities, etc.):** H. Elfandy, F. Pederzoli, K. Viswanathan, A. Vosoughi, M. Blattner, J.M. Mosquera, C. Barbieri, M. Loda

**Analysis and interpretation of data (e.g., statistical analysis, biostatistics, computational analysis):** H. Elfandy, J. Armenia, F. Pederzoli, E. Pullman, N. Pertega-Gomes, N. Schultz, K. Viswanathan, A. Vosoughi, M. Blattner, K.H. Stopsack, J.M. Mosquera, S. Tyekucheva, M. Loda

**Writing, review, and/or revision of the manuscript:** H. Elfandy, J. Armenia, F. Pederzoli, N. Pertega-Gomes, K. Viswanathan, A. Vosoughi, K.H. Stopsack, G. Zadra, K.L. Penney, J.M. Mosquera, S. Tyekucheva, L.A. Mucci, M. Loda

**Administrative, technical, or material support (i.e., reporting or organizing data, constructing databases):** H. Elfandy, E. Pullman, N. Pertega-Gomes, S. Tyekucheva, L.A. Mucci, C. Barbieri

**Study supervision:** C. Barbieri, M. Loda

## Acknowledgments

M. Loda's work is supported by NIH grants RO1CA131945, R01CA187918, DoD PC130716, and P50 CA90381, and the Prostate Cancer Foundation. H. Elfandy's work is supported by The Ministry of Higher Education and Scientific Research (MHESR) in Egypt. We thank Dr. Mark A. Rubin for his support of the SPOP-mutant GEM model, and Lesa Deonarine for technical assistance. We thank the Translational Research Program at WCM, and the WCM SPORE in Prostate Cancer (P50CA211024). This work was supported by: US NCI (K08CA187417-01, P50CA211024-01, and R01CA215040-01, to C. Barbieri), Urology Care Foundation Rising Star in Urology Research Award (to C. Barbieri.), Damon Runyon Cancer Research Foundation MetLife Foundation Family Clinical Investigator Award (C. Barbieri), and Prostate Cancer Foundation Young Investigator Awards (K.H. Stopsack, K.L. Penney, and L.A. Mucci). This research was funded in part through the NIH/NCI Cancer Center Support Grant, P30 CA008748. The Health Professionals Follow-up Study was supported by the NIH (UM1 CA167552). We would like to thank the participants and staff of the HPFS and the PHS for their valuable contributions. In particular, we would like to recognize the contributions of Liza Gazeeva, Siobhan Saint-Surin, Robert Sheahan, and Betsy Frost-Hawes. We would like to thank the following state cancer registries for their help: AL, AZ, AR, CA, CO, CT, DE, FL, GA, ID, IL, IN, IA, KY, LA, ME, MD, MA, MI, NE, NH, NJ, NY, NC, ND, OH, OK, OR, PA, RI, SC, TN, TX, VA, WA, WY. The authors assume full responsibility for analyses and interpretation of these data.

The costs of publication of this article were defrayed in part by the payment of page charges. This article must therefore be hereby marked *advertisement* in accordance with 18 U.S.C. Section 1734 solely to indicate this fact.

Received April 30, 2018; revised August 24, 2018; accepted October 9, 2018; published first October 17, 2018.

Published OnlineFirst October 17, 2018; DOI: 10.1158/1541-7786.MCR-18-0440



## References


1. Gordetsky J, Epstein J. Grading of prostatic adenocarcinoma: current state and prognostic implications. Diagn Pathol 2016;11:25.
2. Epstein JI, Egevad L, Amin MB, Delahunt B, Srigley JR, Humphrey PA. The 2014 international society of urological pathology (ISUP) consensus conference on Gleason grading of prostatic carcinoma: definition of grading patterns and proposal for a new grading system. Am J Surg Pathol 2016;40:244–52.
3. Newcomb LF, Thompson IM, Boyer HD, Brooks JD, Carroll PR, Cooperberg MR, et al. Outcomes of active surveillance for the management of clinically localized prostate cancer in the prospective, multi-institutional Canary PASS cohort. J Urol 2016;195:313–20.
4. Gleason DF. Classification of prostatic carcinomas. Cancer Chemother Rep 1966;50:125–8.
5. Kweldam CF, Wildhagen MF, Steyerberg EW, Bangma CH, van der Kwast TH, van Leenders GJ. Cribriform growth is highly predictive for postoperative metastasis and disease-specific death in Gleason score 7 prostate cancer. Mod Pathol 2015;28:457–64.
6. Chua MLK, Lo W, Pintilie M, Murgic J, Lalonde E, Bhandari V, et al. A prostate cancer "Nimbosus": genomic instability and SChLAP1 dysregulation underpin aggression of intraductal and cribriform subpathologies. Eur Urol 2017;72:665–74.
7. Roobol MJ, Verbeek JFM, van der Kwast T, Kummerlin IP, Kweldam CF, van Leenders G. Improving the Rotterdam European randomized study of screening for prostate cancer risk calculator for initial prostate biopsy by incorporating the 2014 international society of urological pathology Gleason grading and cribriform growth. Eur Urol 2017;72:45–51.
8. Trudel D, Downes MR, Sykes J, Kron KJ, Trachtenberg J, van der Kwast TH. Prognostic impact of intraductal carcinoma and large cribriform carcinoma architecture after prostatectomy in a contemporary cohort. Eur J Cancer 2014;50:1610–6.
9. Kweldam CF, Kummerlin IP, Nieboer D, Verhoef EI, Steyerberg EW, van der Kwast TH, et al. Disease-specific survival of patients with invasive cribriform and intraductal prostate cancer at diagnostic biopsy. Mod Pathol 2016;29:630–6.
10. Cancer Genome Atlas Research Network. The molecular taxonomy of primary prostate cancer. Cell 2015;163:1011–25.
11. Robinson D, Van Allen EM, Wu YM, Schultz N, Lonigro RJ, Mosquera JM, et al. Integrative clinical genomics of advanced prostate cancer. Cell 2015;161:1215–28.
12. Cerami E, Gao J, Dogrusoz U, Gross BE, Sumer SO, Aksoy BA, et al. The cBio cancer genomics portal: an open platform for exploring multidimensional cancer genomics data. Cancer Discov 2012;2:401–4.
13. Gao J, Aksoy BA, Dogrusoz U, Dresdner G, Gross B, Sumer SO, et al. Integrative analysis of complex cancer genomics and clinical profiles using the cBioPortal. Sci Signal 2013;6:pl1.
14. Giovannucci E, Liu Y, Platz EA, Stampfer MJ, Willett WC. Risk factors for prostate cancer incidence and progression in the health professionals follow-up study. Int J Cancer 2007;121:1571–8.
15. Gaziano JM, Sesso HD, Christen WG, Bubes V, Smith JP, MacFadyen J, et al. Multivitamins in the prevention of cancer in men: the Physicians' Health Study II randomized controlled trial. JAMA 2012;308:1871–80.
16. Steering Committee of the Physicians' Health Study Research Group. Final report on the aspirin component of the ongoing Physicians' Health Study. N Engl J Med 1989;321:129–35.
17. Pettersson A, Lis RT, Meisner A, Flavin R, Stack EC, Fiorentino M, et al. Modification of the association between obesity and lethal prostate cancer by TMPRSS2:ERG. J Natl Cancer Inst 2013;105:1881–90.
18. Stark JR, Perner S, Stampfer MJ, Sinnott JA, Finn S, Eisenstein AS, et al. Gleason score and lethal prostate cancer: does $3 + 4 = 4 + 3$? J Clin Oncol 2009;27:3459–64.
19. Pettersson A, Graff RE, Bauer SR, Pitt MJ, Lis RT, Stack EC, et al. The TMPRSS2:ERG rearrangement, ERG expression, and prostate cancer outcomes: a cohort study and meta-analysis. Cancer Epidemiol Biomarkers Prev 2012;21:1497–509.
20. Ahearn TU, Pettersson A, Ebot EM, Gerke T, Graff RE, Morais CL, et al. A prospective investigation of PTEN loss and ERG expression in lethal prostate cancer. J Natl Cancer Inst 2015;108:pii: djv346.
21. Blattner M, Lee DJ, O'Reilly C, Park K, MacDonald TY, Khani F, et al. SPOP mutations in prostate cancer across demographically diverse patient cohorts. Neoplasia 2014;16:14–20.
22. Khani F, Mosquera JM, Park K, Blattner M, O'Reilly C, MacDonald TY, et al. Evidence for molecular differences in prostate cancer between African American and Caucasian men. Clin Cancer Res 2014;20:4925–34.
23. Blattner M, Liu D, Robinson BD, Huang D, Poliakov A, Gao D, et al. SPOP mutation drives prostate tumorigenesis in vivo through coordinate regulation of PI3K/mTOR and AR signaling. Cancer Cell 2017;31:436–51.
24. Ashburner M, Ball CA, Blake JA, Botstein D, Butler H, Cherry JM, et al. Gene ontology: tool for the unification of biology. The gene ontology consortium. Nat Genet 2000;25:25–9.
25. Kanehisa M, Furumichi M, Tanabe M, Sato Y, Morishima K. KEGG: new perspectives on genomes, pathways, diseases and drugs. Nucleic Acids Res 2017;45:D353–61.
26. Liberzon A, Birger C, Thorvaldsdottir H, Ghandi M, Mesirov JP, Tamayo P. The molecular signatures database (MSigDB) hallmark gene set collection. Cell Syst 2015;1:417–25.
27. Shtivelman E, Beer TM, Evans CP. Molecular pathways and targets in prostate cancer. Oncotarget 2014;5:7217–59.
28. Kluth M, Amschler NN, Galal R, Moller-Koop C, Barrow P, Tsourlakis MC, et al. Deletion of 8p is an independent prognostic parameter in prostate cancer. Oncotarget 2017;8:379–92.
29. Williams JL, Greer PA, Squire JA. Recurrent copy number alterations in prostate cancer: an in silico meta-analysis of publicly available genomic data. Cancer Genet 2014;207:474–88.
30. Lotan TL, Carvalho FL, Peskoe SB, Hicks JL, Good J, Fedor H, et al. PTEN loss is associated with upgrading of prostate cancer from biopsy to radical prostatectomy. Mod Pathol 2015;28:128–37.
31. Bowen C, Ju JH, Lee JH, Paull TT, Gelmann EP. Functional activation of ATM by the prostate cancer suppressor NKX3.1. Cell Rep 2013;4:516–29.
32. Markert EK, Mizuno H, Vazquez A, Levine AJ. Molecular classification of prostate cancer using curated expression signatures. Proc Natl Acad Sci U S A 2011;108:21276–81.
33. Barbieri CE, Baca SC, Lawrence MS, Demichelis F, Blattner M, Theurillat JP, et al. Exome sequencing identifies recurrent SPOP, FOXA1 and MED12 mutations in prostate cancer. Nat Genet 2012;44:685–9.
34. Boysen G, Barbieri CE, Prandi D, Blattner M, Chae SS, Dahija A, et al. SPOP mutation leads to genomic instability in prostate cancer. eLife 2015;4:pii: e09207.
35. Rider L, Cramer SD. SPOP the mutation. eLife 2015;4:pii: e11760.
36. Rodrigues LU, Rider L, Nieto C, Romero L, Karimpour-Fard A, Loda M, et al. Coordinate loss of MAP3K7 and CHD1 promotes aggressive prostate cancer. Cancer Res 2015;75:1021–34.
37. Lee WH, Isaacs WB, Bova GS, Nelson WG. CG island methylation changes near the GSTP1 gene in prostatic carcinoma cells detected using the polymerase chain reaction: a new prostate cancer biomarker. Cancer Epidemiol Biomarkers Prev 1997;6:443–50.
38. Friedlander TW, Roy R, Tomlins SA, Ngo VT, Kobayashi Y, Azameera A, et al. Common structural and epigenetic changes in the genome of castration-resistant prostate cancer. Cancer Res 2012;72:616–25.
39. Olkhov-Mitsel E, Siadat F, Kron K, Liu L, Savio AJ, Trachtenberg J, et al. Distinct DNA methylation alterations are associated with cribriform architecture and intraductal carcinoma in Gleason pattern 4 prostate tumors. Oncol Lett 2017;14:390–6.
40. Yang YA, Yu J. EZH2, an epigenetic driver of prostate cancer. Protein Cell 2013;4:331–41.
41. Ramaswamy S, Nakamura N, Vazquez F, Batt DB, Perera S, Roberts TM, et al. Regulation of G1 progression by the PTEN tumor suppressor protein is linked to inhibition of the phosphatidylinositol 3-kinase/Akt pathway. Proc Natl Acad Sci U S A 1999;96:2110–5.
42. Cha TL, Zhou BP, Xia W, Wu Y, Yang CC, Chen CT, et al. Akt-mediated phosphorylation of EZH2 suppresses methylation of lysine 27 in histone H3. Science 2005;310:306–10.
43. Khemlina G, Ikeda S, Kurzrock R. Molecular landscape of prostate cancer: implications for current clinical trials. Cancer Treat Rev 2015;41:761–6.
44. Mateo J, Carreira S, Sandhu S, Miranda S, Mossop H, Perez-Lopez R, et al. DNA-repair defects and olaparib in metastatic prostate cancer. N Engl J Med 2015;373:1697–708.

Published OnlineFirst October 17, 2018; DOI: 10.1158/1541-7786.MCR-18-0440



45. Iczkowski KA, Torkko KC, Kotnis GR, Wilson RS, Huang W, Wheeler TM, et al. Digital quantification of five high-grade prostate cancer patterns, including the cribriform pattern, and their association with adverse outcome. Am J Clin Pathol 2011;136:98–107.
46. Bottcher R, Kweldam CF, Livingstone J, Lalonde E, Yamaguchi TN, Huang V, et al. Cribriform and intraductal prostate cancer are associated with increased genomic instability and distinct genomic alterations. BMC Cancer 2018;18:8.
47. Truong M, Feng C, Hollenberg G, Weinberg E, Messing EM, Miyamoto H, et al. A comprehensive analysis of cribriform morphology on magnetic resonance imaging/ultrasound fusion biopsy correlated with radical prostatectomy specimens. J Urol 2018;199:106–13.
48. Wyatt AW, Azad AA, Volik SV, Annala M, Beja K, McConeghy B, et al. Genomic alterations in cell-free DNA and enzalutamide resistance in castration-resistant prostate cancer. JAMA Oncol 2016;2:1598–606.

AACR American Association for Cancer Research

Molecular Cancer Research

# Genetic and Epigenetic Determinants of Aggressiveness in Cribriform Carcinoma of the Prostate

Habiba Elfandy, Joshua Armenia, Filippo Pederzoli, et al.

*Mol Cancer Res* Published OnlineFirst October 17, 2018.